CHARACTERISTICS OF LANGMUIR TURBULENCE OBSERVED IN SHALLOW WATER

Ann E. Gargett and Judith R. Wells
Center for Coastal Physical Oceanography
Dept. of Ocean, Earth and Atmospheric Sciences, Old Dominion University,
Norfolk, Virginia 23529, USA
gargett@ccpo.odu.edu; jwells@ccpo.odu.edu

ABSTRACT

Recent acoustic observations in shallow coastal waters have provided unique measurements of the properties of both mean and turbulent fields associated with sporadic occurrence of turbulent eddies that develop first near the sea surface as wind forcing increases and eventually engulf the full water column during extended storms. The "large eddies" of this turbulent field exhibit many of the features described as characteristic of Langmuir circulations, modified by the presence of a bottom boundary. Several diagnostics accessible to the observational data agree with results of associated LES of turbulence in a surface-stress-driven Couette flow when the Langmuir vortex forcing term is included. A particularly sensitive diagnostic, the depth trajectory of Lumley invariants, is strikingly different for Langmuir and non-Langmuir turbulence.

INTRODUCTION

In April 2003, a 5-beam "turbulence" VADCP (Vertical-beam Acoustic Doppler Current Profiler) was installed on a stable bottom platform at a node of LEO-15, a cabled ocean observatory off the coast of New Jersey. The special vertical beam of the VADCP provided unambiguous measurement of vertical velocity w from ~1 m above the seabed up to the sea surface. Slant-beam pairs provided standard estimates of horizontal velocity components, subject to loss of the upper ~15% of the water column through signal contamination by sidelobe returns, and to the (spatial) filtering effect of beam spread (for details, see Gargett et al., 2004). Full water-column profiles were acquired roughly every second from April 15 to October 31, an extended deployment that covered the full annual range of water column stability, tidal and atmospheric forcing. Ancillary data include thermistor chain measurements which, coupled with sporadic CTD profiles at the LEO node, provide essential information on water column stratification, and a full suite of meteorological forcing fields. Amid a wealth of turbulent processes present in this data, the most striking were episodes of Langmuir circulations (LC) that achieve vertical scales equal to the water depth under extended storms (Gargett et al., 2004): these are termed Langmuir supercells (LSC) because of their profound effects on sediment resuspension and transport.

The present paper describes the observational data on LSC that underlie a comparison between field observations of Langmuir turbulence in the ocean and large-eddy simulations carried out to emulate them, simulations described in a companion paper by Tejada-Martínez and Grosch (2005: henceforth TMG) in this volume. This comparison is limited by various observational constraints (besides the instrumental limitations mentioned above) that do not affect the computations. The real-world observations took place in a complex environment that includes tidal flows and may include rotational effects in addition to the uni-directional (wind) stress-driven mean flow of the simulations. Because of the tides, neither fluid depth nor "mean" flow is constant in time. Surface gravity waves produce high-frequency variability that must be (time) filtered out of the observed fluid velocities. The fact that the filtering process leaves only turbulent structures with horizontal spatial scales larger than several meters is not a major constraint, since dependable horizontal velocities can only be derived from the slant beam pairs for structures with horizontal scales significantly larger than the spatial spread of the beams, of O(H) at the water surface in water of depth H. However such filtering can only be carried out with time-continuous records, hence at depths below a minimum height above bottom that decreases as surface wave heights increase. Thus the near-surface region inaccessible to measurements increases in depth during high winds/seas. We also cannot measure flow very near the solid bottom boundary (which itself is neither exactly solid nor constant with time), because of the finite size of the VADCP. Finally, the observed fields can be averaged only in time, not in time and (assumed statistically homogeneous) horizontal flow dimensions. Despite all of these constraints, many of the characteristic features of LSC observations agree, both qualitatively and often quantitatively, with LES results carried out using stress and surface wave parameters derived from the observational conditions.

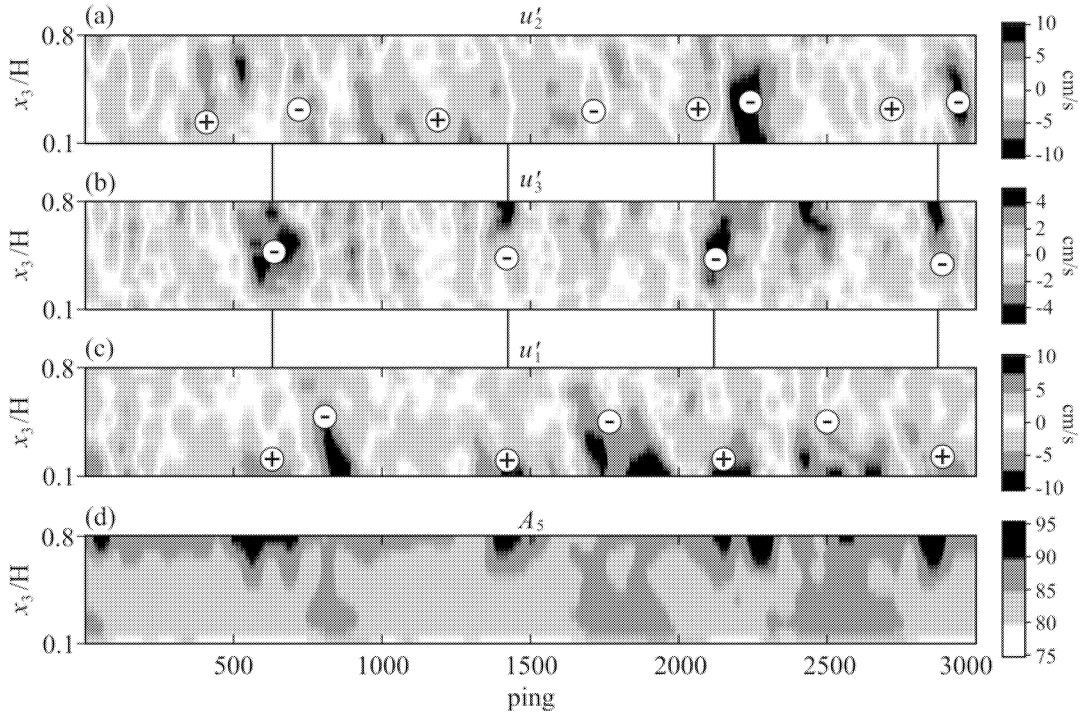

Figure 1: Fields of (u_1', u_2', u_3') = downwind, crosswind, and vertical fluctuating water velocity components (in cm/s), and of backscatter amplitude A_5 (in relative units), as measured by an upward-looking vertical-beam acoustic Doppler current profiler deployed in 15m of water during an extended storm off the coast of New Jersey. Vertical coordinate x_3 is scaled by mean water depth H = 15.1m over a record length of ~2.2 hours: the data shown is a subset corresponding to ~ 66 minutes. Vertical lines between panels mark the centers of the downwelling limbs of Langmuir cells. A more easily interpreted color version of this figure can be accessed via http://www.ccpo.odu.edu/~jwells/TSFP4_GWSupp.pdf. See also Fig.2 of Gargett et al., (2004).

OBSERVATIONAL FEATURES

Figure 1 shows fields of measured fluctuation velocity components (u_1', u_2', u_3') in the coordinate system (x_1, x_2, x_3) = (downwind, crosswind, vertical) during an episode of LSC. The three-dimensional fluctuation velocity field[1] reveals many flow features normally considered typical of LC (Smith et al., 1987; Weller and Price, 1988; Thorpe, 2004) as cartooned for shallow water in Fig.2. Downwelling ($u_3' < 0$) regions are narrower than upwelling regions; maximum downwelling velocities are found at mid-depth, and exceed maximum upwelling velocities. Characteristic downwind "jets" ($u_1' > 0$, Fig.1c) are centered under downwelling regions. At the time of these measurements, the mean water velocity $< \underline{u} >_t$ was slightly to the left of the wind stress (as shown in Fig.2), producing cross-wind drift ($< u_2 >_t$) of Langmuir cells past the fixed VADCP such that, as a downwelling region approaches, the horizontal cross-wind component near the bottom should first be positive, then switch to negative at the center of a downwelling ($< u_3' >_t$). This relationship between $< u_3' >_t$ and $< u_2' >_t$ is clearly observed in Fig.1a,b. Observed $< u_2' >_t$ does *not* clearly reveal expected convergent crosswind flow as the surface is approached, because the upper 30% of the mean water column could not be sampled during this period of large surface waves. However, lack of strongly convergent flow in the sampled domain implies that the actual convergent flow is surface-intensified, another characteristic of LC. Unlike LC observed in deep water, both positive and negative flow variations along the x_1 axis are observed to be strongly intensified towards the bottom. The bottom panel of Fig.1 shows A_5, the backscatter amplitude measured by the vertical beam. Clouds of high backscatter originating near the surface are caused by air microbubbles, injected into

[1] Horizontal fluctuating velocities in each (height) bin have been calculated by removing a linear least squares fit to the velocities in each measurement bin of a record, typically ~ 2.2 hours long . This method of removing low-frequency (tidal) variation of the "mean" produces results that are almost identical to those resulting from a more complex procedure that removes periodic least squares fits to 5 dominant tidal frequencies.

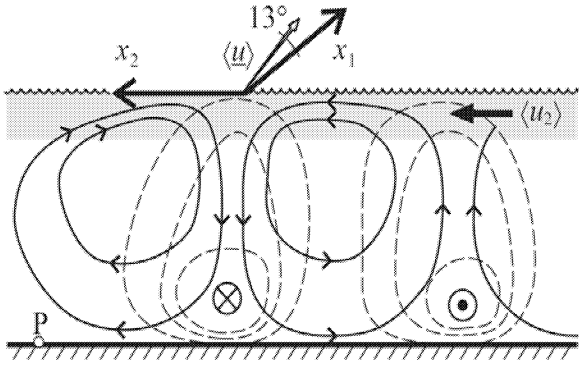

Figure 2: Basic features of Langmuir circulations in shallow water, shown with the geometry of wind stress $\underline{\tau}$, parallel to x_1, and mean current $< \underline{u} >$ at the time of the record in Fig.1.

the surface layer by breaking waves, being advected to depth in the downwelling phase of LC. High backscatter originating from the bottom (Fig. 1d) suggests bottom sediment being delivered to the overlying LC and carried high into the water column by the upward-going limbs of the cells.

TMG (their Fig.3,4) demonstrate dramatic differences between flow patterns characteristic of surface-stress-forced unstratified Couette flow and of that same flow with the addition of the Langmuir vortex forcing term. Examination of the flow structures obtained from their LES that include Langmuir forcing derived from observed surface stress and surface wave parameters at the time of Fig.1 shows features that are in remarkable agreement with observations (and absent from basic Couette flow): specifically, strong bottom intensification of $< u_1' >_t$, a mid-depth maximum in downwelling velocities, and a scale ratio of upwelling to downwelling limbs of 1.6, compared with 1.5 from observations. Another comparison is seen in Fig.3, which shows profiles of (a) mean horizontal velocities in downwind $< u_1 >_t$ and crosswind $< u_2 >_t$ directions, (b) turbulent velocity variances $< u_i' u_i' >_t$ and (c) turbulent stresses $- < u_i' u_j' >_t$, with respect to height above bottom x_3 non-dimensionalized by mean water depth H = 15.1m. Velocities are normalized by mean downwind velocity at mid-channel, U_c = 30.3 cm/s. The ~2.2 hour period of time averaging (denoted by subscript 't') contains several large time eddy scales. Fig.3 (d-f) shows the same variables computed by the LES, averaged over both time and horizontal planes. Many of the observational features are similar in both shape and magnitude to the computational results. Differences include larger crosswind velocity variance and non-zero $- < u_1' u_2' >_t$ and $- < u_2' u_3' >_t$ shear stress components, all of which may

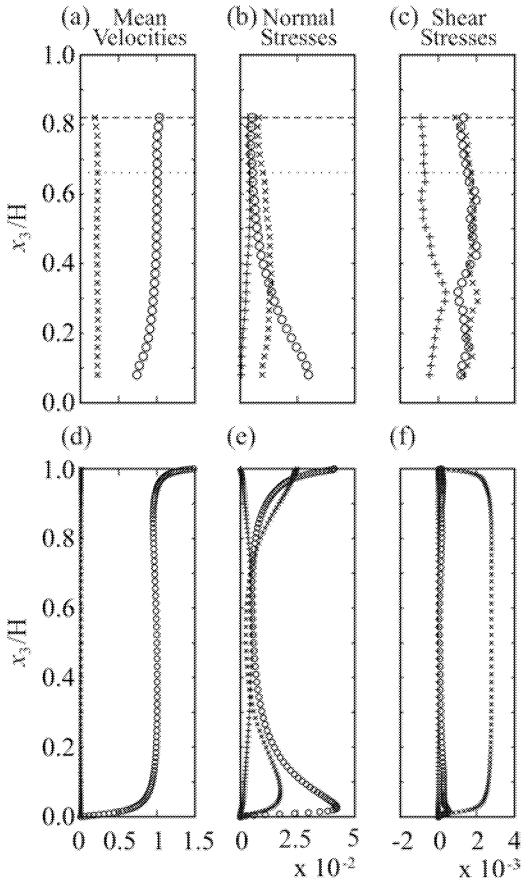

Figure 3: Profiles with respect to height above bottom x_3, non-dimensionalized by mean water depth H. (a) Mean horizontal velocities in the downwind (o = $< u_1 >_t$) and crosswind (x= $< u_2 >_t$) directions, (b) turbulent normal stresses (velocity variances) (o=V_{11}, x =V_{22}, + = V_{33}) and (c) shear stresses (o=S_{12}, x=S_{13}, +=S_{23}), where V_{ii} and S_{ij} are as defined in the caption to Table 1. Velocities are normalized by U_c , the mean downwind velocity at mid-channel. The averaging period of ~2.2 hours, which includes the data shown in Fig.1, contains several large time eddy scales. (d-f) Same fields calculated from LES, averaged over time and horizontal plane.

be associated with the presence of a small crosswind mean velocity (which may be due to tides or pressure gradients) in the observations that is absent from the LES.

Since Fig.3(a) is a single realization of a complex turbulent flow, we also examine variability in the observational estimates of the second-order turbulent quantities. Fig.4 shows ensemble averages and standard deviation error bars for turbulent velocity variances (normal stresses) and shear stresses over an ensemble consisting of 8 time-consecutive realizations like that shown in Fig.3(a): time and depth-

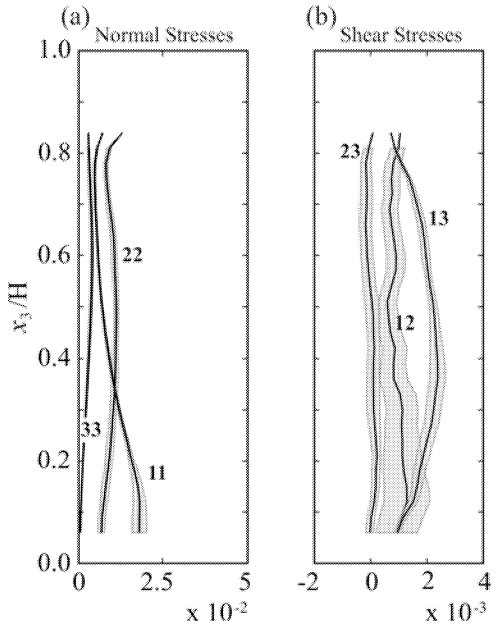

Figure 4: Ensemble averages and standard deviation error bars for turbulent (a) normal stresses (velocity variances) V_{ii} and (b) shear stresses S_{ij} , where V_{ii} and S_{ij} are defined in the caption to Table 1: curves are labeled by ii or ij values. The ensemble consists of 8 time-consecutive realizations like that shown in Fig.3, under conditions of approximately constant wind stress of ~0.1 N/m^2.

averaged turbulence statistics for all realizations are found in Table 1. While wind stress remained approximately constant in both magnitude (~0.1 N/m^2) and direction (~245°) throughout this 18 hour period, tidal variability caused crosswind velocities to vary from 3 to 19.7 cm/s. Despite this variability in crosswind currents, the ensemble mean variances are not highly variable, hence the excess crosswind variance appears robust. However the ensemble mean $-<u_2'u_3'>_t$ shear stress component has zero average, in agreement with the LES. The $-<u_1'u_2'>_t$ stress component has large error bars, especially near bottom, but still appears to have a significant positive ensemble mean value. The ensemble mean $-<u_1'u_3'>_t$ stress component dominates the other two stress components, although it is less uniform in the vertical than either the LES or the single realization shown in Fig.3a.

The final diagnostic we present is the depth trajectory or map of Lumley invariants (Lumley, 1978), calculated over the part of the water column accessible to the observations, and plotted in the Lumley "triangle" within which realizable turbulent flows must lie: the form shown in Fig.5 is that used by Pope (2000). The Lumley invariant map (built using

file	U_C	V_{11}	V_{22}	V_{33}	R_{21}	R_{31}	S_{12}	S_{13}	S_{23}
23	28.7	7.7	7.5	3.1	0.97	0.40	-0.3	+1.9	+0.1
24	30.4	11.0	10.2	2.7	0.93	0.25	+1.4	+2.0	-0.6
25	30.7	11.5	10.5	3.6	0.91	0.31	+2.3	+2.3	-0.2
26	26.8	8.5	8.1	2.1	0.95	0.25	+1.5	+1.5	+0.5
27	31.1	8.2	6.7	1.6	0.82	0.20	-0.6	+1.5	+0.6
28	29.9	8.1	8.9	1.5	0.85	0.19	+0.06	+1.2	+0.3
29	29.8	7.4	8.9	2.4	1.2	0.32	+0.6	+1.4	-0.04
30	29.1	8.5	11.0	2.5	1.3	0.29	+2.0	+1.6	-0.5

Table 1: Turbulence statistics averaged over depth and time for files of length ~ 2.2 hours spanning several large eddy periods: all velocities are in cm/s. U_c is mean downwind velocity at mid-depth at the time of the file. Values in the table are depth averages of $V_{ii} = <u_i'u_i'>_t$, $S_{ij} = -<u_i'u_j'>_t$, and $R_{i1} = <u_i'u_i'>_t / <u_1'u_1'>_t$.

$II = b_{ij}b_{ji}$ and $III = b_{ij}b_{jk}b_{ki}$, two of the three invariants of the turbulence anisotropy tensor $b_{ij} = <u_i'u_j'> / 2k - \delta_{ij}/3$ where $k = <u_i'u_i'>/2$ is the resolved turbulent kinetic energy) is extremely sensitive to the underlying flow structures. Normal turbulent boundary layers have a depth trajectory that begins (at the wall) along the upper curved boundary, then moves first towards the upper right corner, then down along the righthand boundary of the triangle as distance from the wall increases. Surface-stress-forced LES (see TMG) and observational data without LC (not shown) both reproduce this behaviour. The trajectory of the LSC observations is a startling contrast, beginning near the upper boundary, but curving outwards towards the lefthand triangle boundary before turning back towards the righthand boundary. While individual realizations (Fig.3a-c) differ in details, they all have this characteristic "C" shape. The observations differ in some details from the LES results of TMG. Mid-channel values approach but are not found right on the righthand boundary, and the observational trajectory doubles back towards the lefthand boundary, as they observe, only if we include data within the 15% of the mean water column depth that may potentially be contaminated by sidelobe reflections. Fig.5 includes such data because we see no obvert signs of sidelobe contamination in these records. Despite these caveats, the major change of character of the depth trajectories of Lumley invariants between flows and simulations with and without LC appears robust.

CONCLUSIONS

Langmuir supercells are an important mechanism for the transport of sediment and bioactive materials in shallow coastal oceans, and as such are of practical as well as scientific interest. Field observations of Langmuir turbulence

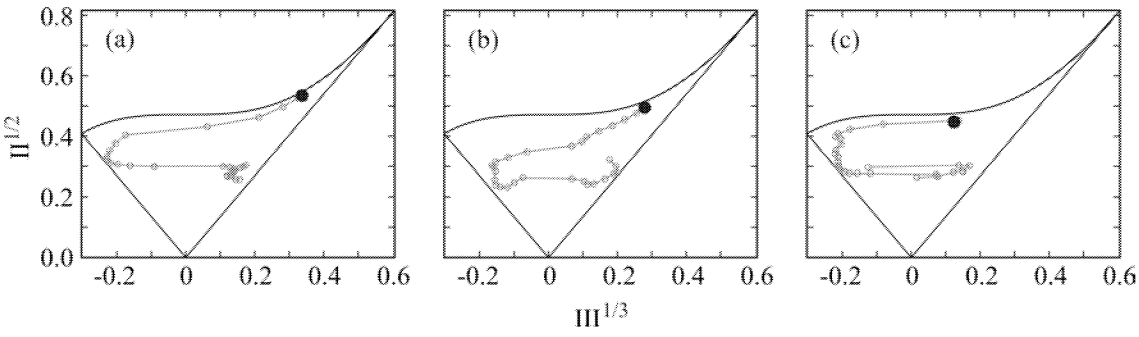

Figure 5: The depth trajectory of Lumley invariants for 3 consecutive records, each of ~2.2 hours duration: the solid black point marks the measurement level closest to the ocean bottom. Filtering of the original data truncates the turbulent kinetic energy spectrum at frequencies slightly above those corresponding to the beginning of a range with roughly -5/3 spectral slope, corresponding to scales similar to those resolved by the associated LES (see TMG).

have many characteristics in common with LES of surface-stress-driven Couette flow, provided the Langmuir vortex forcing term is included. Differences in details may result from the existence in the observations of a mean crosswind velocity, absent in the simulations. Agreement is nevertheless sufficiently good to encourage turbulence modeling, using the results of the Langmuir LES, as means of incorporating the major effects of Langmuir turbulence into models of the shallow coastal ocean.

ACKNOWLEDGMENTS

We are grateful for research support from NSF (grant OCE-136403) and NOAA (grant NA06RU0139), and generous support from S. Glenn, O. Schofield and E. Creed. The success of the LEO-15 deployment was due to R. Petrecca and staff of the Rutgers Marine Field Station, and the technical expertise of C. Powell. S. Huang provided essential data handling and access programming.

REFERENCES

Gargett, A., Wells, J., Tejada-Martínez, A. E., and Grosch, C. E., 2004, "Langmuir supercells: a mechanism for sediment resuspension and transport in shallow seas", *Science*, Vol. 306, pp.1925-1928.

Lumley, J. L., 1978, "Computational modeling of turbulent flows", *Adv. Appl. Mech.*, Vol.18, pp.123-176.

Pope, S. B, 2000, *Turbulent Flows*, Cambridge University Press, Cambridge, UK. 771pp.

Smith, J., Pinkel, R. and Weller, R. A., 1987, "Velocity structure in the mixed layer during MILDEX", *J. Phys. Oceanogr.*, Vol.17, pp. 425-439.

Thorpe, S. A., 2004, "Langmuir circulation", *Annu. Rev. Fluid Mech.*, Vol. 36, pp. 55-79.

Tejada-Martínez, A. E. and Grosch., C. E., 2005, *Proceedings, Turbulence and Shear Flow Phenomena 4*, Williamsburg, Virginia, USA.

Weller, R A. and Price, R. A., 1988, "Langmuir circulation within the oceanic mixed layer", *Deep-Sea Res.*, Vol. 35, pp. 711-747.